V European Conference on Computational Fluid Dynamics
ECCOMAS CFD 2010
J. C. F. Pereira and A. Sequeira (Eds)
Lisbon, Portugal, 14-17 June 2010

FINITE ELEMENT SIMULATIONS OF COLLOIDAL AGGREGATES UNDER SHEAR FLOW CONDITIONS

Eva C. Schlauch*, Volker Becker†, Marek Behr*, Heiko Briesen‡

*RWTH Aachen University, Chair for Computational Analysis of Technical Systems (CATS),
Center for Computational Engineering Science (CCES),
Schinkelstr. 2 D-52062 Aachen
e-mail: {schlauch,behr}@cats.rwth-aachen.de
†Max Planck Institute for Dynamics of Complex Technical Systems,
Sandtorstr. 1, D-39106 Magdeburg
e-mail: becker@mpi-magdeburg.mpg.de
‡Center of Life and Food Sciences Weihenstephan, Technische Universität München,
Weihenstephaner Steig 23, D-85350 Freising
e-mail:briesen@wzw.tum.de

Key words: colloidal aggregates, finite element simulations, discrete element method, mechanistic model

Abstract. *We perform finite element simulations of aggregates in shear flow environments, in order to improve the model of hydrodynamic forces used for discrete element simulations. The mechanistic model for the discrete element simulations implies until now the so-called free-draining approximation for the fluid forces which is a drastic simplification. From the finite element simulations we extract the fluid forces acting on the constituents of small aggregates of 8 to 20 particles. With these highly-resolved results we can extract parameters for the hydrodynamic force model. We find two major results: first, inside the aggregates the fluid flow is relaxed and can for the small aggregates be parameterized by an effective shear rate which is significantly smaller than the ambient shear rate, while for the large aggregates, a core-shell model is proposed; and second, the flow field in the core region of the aggregates is not aligned with the external flow, which is the case for the forces acting on the shell particles.*

1 INTRODUCTION

Colloidal aggregates appear in different areas of chemical process engineering. They form from nano- or micro-particles in suspensions such as gels or ointments. Their structure is of major importance in the rheology of these suspensions, and it is already well-known in resting fluids. However, under process conditions, shear forces act on the aggregates, and the fluid forces significantly affect the aggregate structure. It is difficult to perform experiments that yield information about the restructuring of particle clusters in shear flow environments typical for the named processes. It appears therefore to be suitable, to apply simulations to investigate the restructuring in these multi-phase flows.

We want to perform discrete element simulations (DEM) of colloidal aggregates and need a model to describe the forces acting in these particle systems. In general, one must distinguish between the hydrodynamic and the particle interaction forces. In this work, we want to concentrate on the hydrodynamic interaction. For current DEM simulations, it is popular to use the free-draining approximation (cdf. [7, 8, 9, 16, 17]) which neglects the influence of neighboring particles in the fluid flow. In the Stokesian dynamics approach (cf. [6, 18]), the influence of the neighbors is incorporated in form of the mobility matrix. In this way, each particle is represented by its first few multipoles regarding the hyrodynamic interaction. Other approaches use geometrical descriptions for the computations of hydrodynamic forces, such as in Higashitani et al. [14], or in Fanelli et al. [11, 12].

Depending on the process conditions, colloids can be more or less compact. This property can be parameterized by the fraction of volume that is filled by the aggregate. It is expected that different volume fractions lead to different restructuring behavior. It has been shown by means of Stokesian dynamics simulations, that compact aggregates will undergo restructuring while less dense structures will experience breakup (cf. [13]).

In this work, we describe our first steps to provide a more detailed mechanistic model for the hydrodynamic forces. These forces can be extracted from finite element simulations. We show results for small aggregates containing up to 20 constituent particles and of three different volume fractions under steady shear flow conditions. From the results we obtain parameters for the fluid forces which will lead to a more precise modeling. Eventually, such mechanistic modeling will allow to effectively control the structure and final size of colloidal aggregates by exposing them to a well-defined hydrodynamic environment and thus control the suspension behavior.

2 MODELING

We consider for the DEM simulations a mechanistic model. In this model we assume that the primary particles are of spherical shape and that the solvent has a high viscosity such that particle Reynolds numbers are small ($Re \ll 1$). One may distinguish in this model the forces acting between particles and the hydrodynamic forces. The former can be called internal forces while the latter may be considered as external forces and cause aggregate restructuring or breakup.

The internal forces are incorporated in our model by means of the Derjaguin, Landau, Verwey and Overbeek theory (DLVO, see for example [10]). This theory combines the effects of van der Waals attraction and repulsive electrostatic double layer forces. We added a repulsive short-range potential (Born repulsive force) to make sure that particles cannot overlap. These three components, van der Waals, electric double layer, and Born forces, depend on the center-center distance of the particles, ie., they act parallel to the bond. For the forces acting perpendicular to the bond, we introduced tangential forces and torques with a spring-rod model. This has been described in more detail in [1, 2].

The hydrodynamic forces appear in our mechanistic model in the form of the free-draining approximation. In the framework of this approximation, the forces acting on each particle in the fluid are given by the Stokes drag which is defined for a single spherical particle immersed in an unbounded fluid with a uniform flow velocity. As found in standard textbooks (see e.g., [15]), a formulation of the Stokes drag force acting on particle i is given by:

$$\boldsymbol{F}_{\mathrm{Drag},i} = 6\pi\eta a \left(\boldsymbol{v}_i - \boldsymbol{u}\right) \ , \tag{1}$$

with η, a, $\boldsymbol{v}_i$ and $\boldsymbol{u}$ being the dynamic viscosity of the carrier fluid, the particle radius, the velocity of the i'th particle, and the fluid velocity, respectively. Using the free-draining approximation implies, that the influence of neighboring particles on the fluid flow is neglected. In the present case, we choose the reference system to be attached to the particle, that is $\boldsymbol{v} = 0$. Under shear flow conditions we also have to make a decision on the fluid velocity. We choose for the fluid velocity acting on particle i that velocity which would act at the position of the particle's center $\boldsymbol{r}_i$: $\boldsymbol{u} = \boldsymbol{u}(\boldsymbol{r}_i)$. In this way, we also neglect the different fluid velocities acting at different points on the particle surface. Moreover, due to the fact that we neglect the influence of neighboring particles, all forces are parallel to the fluid flow.

3 SIMULATION METHOD

As a first step to develop a more detailed model for the hydrodynamic forces acting on the aggregate and its constituents, we perform steady simulations of the fluid flow arround different aggregates. The aggregates are centered in the origin of the computational domain and are surrounded by a cubical volume of fluid. Inside the fluid volume an external flow field with a shear rate is imposed as indicated in Figure 1. The fluid volume is discretized using a tetrahedral unstructured mesh. This is performed by first triangulating the surfaces of the geometry, where the surfaces of the primary particles are covered with about 10,000 triangles each, and then using a tetrahedral mesh to fill the volume. Since the fluid flow, for particle Reynolds numbers near zero, is assumed to be sensitive to all boundaries, we investigate this influence in more detail. We discuss this subject in Section 4. The present meshes contain up to 20 million tetrahedra for the larger aggregates which is mainly due to the necessary high resolution of the primary particles. The large number of mesh elements is the main reason why it is impractical,

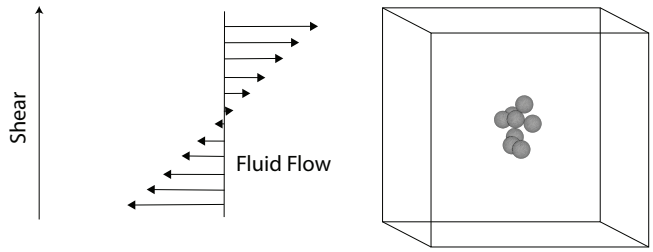

Figure 1: Sketch of the simulation domain. The aggregate is centered at the origin and the surrounding fluid volume is a cube. The shear flow is set at the inflow in the manner indicated by the arrows.

with the current computational tools, to perform simulations of real life aggregates which comprise several thousand particles.

On the finished volume meshes we perform simulations with a finite element solver (cf. [4, 5]). We use approximately 10,000 triangular elements to discretize each of the primary particles' surfaces in order to get an accurate description of the pressure distribution. We solve the steady Stokes equations which might be stated as follows for the domain Ω and its boundary Γ:

$$\begin{aligned} -\nu\boldsymbol{\nabla}^2\boldsymbol{v} + \boldsymbol{\nabla}p &= \boldsymbol{b} && \text{in } \Omega && \text{(equilibrium)},\\ \boldsymbol{\nabla}\cdot\boldsymbol{v} &= 0 && \text{in } \Omega && \text{(incompressibility)},\\ \boldsymbol{v} &= \boldsymbol{v}_D && \text{on } \Gamma_D && \text{(Dirichlet b.c.)},\\ -p\boldsymbol{n} + \nu(\boldsymbol{n}\cdot\boldsymbol{\nabla})\boldsymbol{v} &= \boldsymbol{t} && \text{on } \Gamma_N && \text{(Neumann b.c.)}. \end{aligned}$$

Here, $\boldsymbol{v}$ describes the fluid velocity, $\boldsymbol{v}_D$ the prescribed velocities on the Dirichlet portion of the boundary and p the pressure. The vector $\boldsymbol{n}$ denotes the surface normal of the boundary, ν denotes the kinematic viscosity $\nu = \eta/\rho$ where η is the fluid viscosity and ρ its density. $\boldsymbol{t}$ is a so-called "pseudo-traction" of the boundaries, while $\boldsymbol{b}$ is a body force. The boundary conditions are discussed in Section 4 and the values for density and viscosity are given in Table 1. The particle Reynolds number is $Re = 3.675 \cdot 10^{-3}$. The formulation of the mathematical problem is closed by the equation for the stress tensor $\boldsymbol{\sigma}$ given as follows:

$$\boldsymbol{\sigma} = -p\boldsymbol{I} + \boldsymbol{\tau}, \tag{2}$$

where the first term denotes the hydrostatic stress and $\boldsymbol{\tau}$ the deviatoric stress given as:

$$\tau_{ij} = \eta\left(\frac{\partial v_i}{\partial x_j} + \frac{\partial v_j}{\partial x_i}\right) . \tag{3}$$

The Stokes problem is solved for the fluid velocity and pressure. Simulations are performed on 64 processors using a parallelized version of the solver.

We compute from the pressure on the surfaces the total forces acting on each particle in the aggregates. The hydrodynamic force acting on the i'th particle is given by a sum

over forces acting on its surface elements. For each element of the particle's surface, the force can be calculated as the integral over the element area $\Omega^{(e)}$:

$$f_i^{(e)} = \int_{\Omega^{(e)}} (-p\delta_{ij} + \tau_{ij})\, \hat{n}_j^{(e)} d\Omega \,, \tag{4}$$

where $\hat{n}^{(e)}$ is the element surface normal vector, and δ_{ij} denotes the Kronecker delta distribution. With this scheme, not only the drag can be calculated, but a force vector can be given for a 3-dimensional fluid force.

4 BOUNDARY CONDITIONS AND FINITE SIZE EFFECTS

The sensitivity of the hydrodynamic forces to the presence of artificial boundaries can in principle be high under the low particle Reynolds number or creeping flow condition. The boundary conditions in the present simulations are no-slip for the particle surfaces, shear flow for the inflow, and parallel flow for the walls. On the one hand, the no-slip or stick boundary condition for the aggregates leads to a natural zero flow velocity, while on the other hand the parallel flow for the walls leads to an unnatural constraint. The artificial walls result in a disturbance of the flow field which is felt at the position of the aggregate and which is reduced as the distance to the walls increases.

Since the free-draining approximation applies in principle to spherical particles immersed in a uniform flow field, we start our investigation of the influence of artificial walls with the simulation of a single particle under uniform external flow for different sizes of the surrounding fluid volume. We find a direct dependence of the calculated drag force on the size of the surrounding fluid volume. The result is shown in Figure 2 (a). By contrast, we find a significantly lower wall influence for shear flows acting on aggregates (cf. Figure 2 (b)). In the plots, R indicates the ratio of volume size to particle size, and volume size to aggregate size, respectively. The particle size is a and the aggregate size is taken to be the largest extent of the aggregate. The curves have been fitted using a function of the shape given in Equation (5):

$$f(R) = \frac{c_1}{c_2 + R} + c_3 \,, \tag{5}$$

where the c_i are constants. The good quality of these fits shows that the influence of the artificial walls behaves approximately as $1/R$.

We conclude that the shear forces acting within the fluid, together with the presence of neighboring particles in the aggregate, screen the effect of the artificial walls enough to confine the simulations to a modest fluid volume. We had chosen for the generation of our meshes a volume size ratio of $R = 60$ which, according to Figure 2 (b), does not introduce artefacts from the artificial walls. Furthermore, for future simulations, we may select the value for the ratio R as low as ten without introducing artificial wall effects.

From Figure 2 (a) we can conclude that the drag force on a spherical particle in a fluid volume depends strongly on the presence of other boundaries. One can already at this

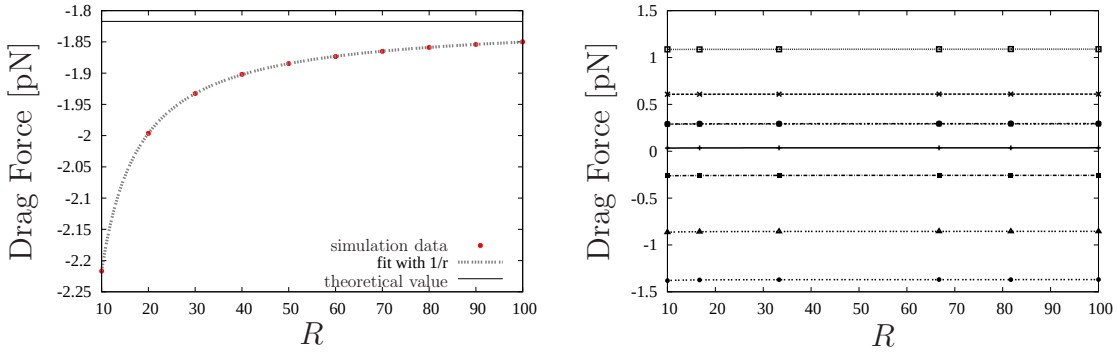

Figure 2: Influence of the artificial walls on the flow field at the position of (a) a single spherical particle in a uniform flow, and (b) a complete aggregate of 8 particles under shear flow conditions. We show the drag force on each particle: one particle in (a), eight particles in (b). For a single particle, we can give a theoretical value for the drag from the Stokes drag force. This is not possible for the aggregate. Nevertheless, it can be clearly seen, that the value for the single particle in a uniform flow will converge only slowly with the theoretical value while we find no significant change in the drag forces for the constituents in the aggregate.

point understand that the introduction of neighboring particles will significantly influence the drag force on each of the particles.

5 SIMULATION RESULTS FOR STEADY CASES

Steady simulations are performed for two different sizes and three different types of aggregates. The general type of aggregates under consideration is constructed in a randomized approach with reaction-limited aggregation (RLA, cf. [19]). With this approach we are able to construct colloidal aggregates of different compactness. The reaction limiting the aggregation is characterized by a sticking efficiency ϵ, by which we describe the probability of each particle to stick to another. A lower probability will ensure compact aggregates, while a higher probability will provide us with bigger yet less dense structures (which can be observed in Figure 3). The three types of aggregates can be distinguished by their sticking efficiency of 1.00, 0.10, and 0.01, respectively.

We prepare ten aggregates of each type containing 8 primary particles and repeat this for a second size of 20 particles per aggregate. Simulations are performed under the settings given in Table 1. We use the same mesh for three simulations and adjust the inflow and outflow to appropriate walls, and change the shear direction. A typical resulting pressure distribution is shown for two large aggregates of different type (sticking efficiency of 0.01 and 1.00) in Figure 3. In the figures, the flow has a velocity gradient from top to bottom such that the flow is from left to right at the top and from right to left at the bottom. The highest pressure values are found at the outermost particles in both cases according to the higher flow velocities. In the following we describe the finite

Parameter	Variable	Value
number of primary particles	N	8, 20
particle diameter	a	735 nm
shear rate	G	50 s^{-1}
fluid density	ρ	1000 kg/m^3
fluid viscosity	η	0.001 kg/ms

Table 1: Aggregate and fluid parameters applied in the simulations.

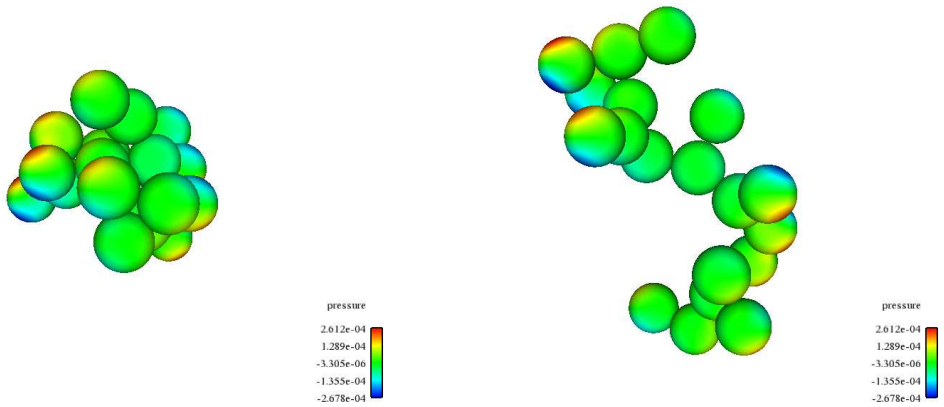

(a) (b)

Figure 3: Pressure distribution on the surfaces of two aggregates of different compactness as calculated by the finite element simulations: RLA aggregate with sticking efficiency of (a) $\epsilon = 0.01$ and (b) $\epsilon = 1.00$. Both aggregates contain the same number of primary particles (20). Unit of pressure is $[nNm^{-2}]$.

element simulation results for both sizes of aggregates.

5.1 Aggregates comprising 8 particles

Due to the shear rate of the applied external fluid flow, the hydrodynamic forces acting on a particle inside the aggregate should depend on its position along the shear axis as the force is related to the relative velocity of external flow and particle. We do in fact find in our simulations a clear correlation between the drag forces on the constituents of the aggregates on the one hand and the position in the direction of the velocity gradient (shear direction) on the other hand (cf. Figure 1). This can be seen in Figure 4 for the three aggregate types. We do a least-squares fit on the data. The slope from the fit can be used to determine an effective shear rate, where we reformulate the free-draining formulation of the drag forces under shear flow conditions as follows (cf. Equation (1)):

$$F_{x,i} = 6\pi\eta a G_{\mathit{eff}} z_i \ . \tag{6}$$

Here, z_i denotes the position of particle i in the direction of the velocity gradient, $F_{x,i}$ the drag force acting on particle i along the flow direction x, and G_{eff} the effective shear rate. Equation (6) can be rearranged to gain an equation for G_{eff}:

$$G_{\mathit{eff}} = \frac{m}{6\pi\eta a} \,, \tag{7}$$

where m denotes the slope extracted from the data. For all three aggregate types we find that the effective internal shear rate, extracted from the slope by Equation (7), is smaller than the external shear rate. The values are given in Table 2. The error bounds

G	$50.0\ s^{-1}$
G_{eff} for $\epsilon = 1.00$	$42.62\ s^{-1} \pm 1.4\%$
G_{eff} for $\epsilon = 0.10$	$44.31\ s^{-1} \pm 1.7\%$
G_{eff} for $\epsilon = 0.01$	$42.67\ s^{-1} \pm 1.6\%$

Table 2: Effective shear rates as extracted with a least-squares fit from the simulation data. The values cannot be distinguished from each other clear enough. Nevertheless, all three of them are significantly smaller than the external shear rate. This implies a shielding effect of the fluid flow inside the aggregate from the external flow.

of all three values overlap, which means that we cannot clearly distinguish them one from another. We expect the effective shear rate to be smaller for compact aggregates than for less dense structures. This effect is probably not visible here, because the aggregates are very small.

5.2 Aggregates comprising 20 particles

The larger aggregates exhibit the same clear correlation between drag force and position along shear direction. But for these aggregates, another effect can be observed which we interpret as a shielding of the core region of the aggregate. As it is shown in Figure 5, in all three data sets there is a lower slope in the core region of the aggregates than in the outer regions. The lower slope indicates lower forces in this core region and thus a shielding by the outer particles from the external fluid flow. A second result, which is caused by the presence of neighboring particles in the flow, is the fact that the hydrodynamic force can have a component perpendicular to the external flow. When this effect is taken into account for the model, it will lead to a different restructuring behavior than just drag forces. As an example, the result for aggregates with $\epsilon = 1.00$ is shown in Figure 6, where we plot the absolute value of the force components for each of the primary particles. One observes that for larger radii, the drag forces outweigh the perpendicular forces. But in the core region the perpendicular force components cannot be neglected in the hydrodynamic force model. This holds for aggregates of $\epsilon = 0.10$ and $\epsilon = 0.01$ as well.

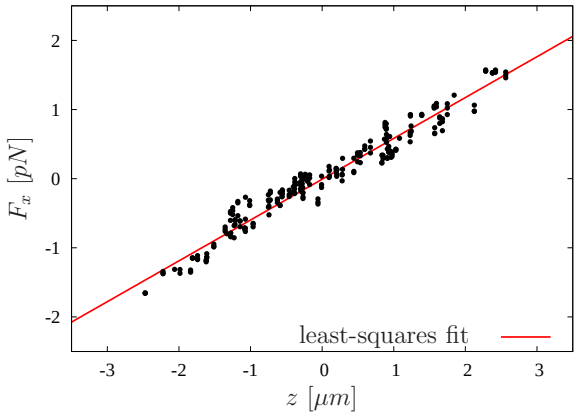

(a)

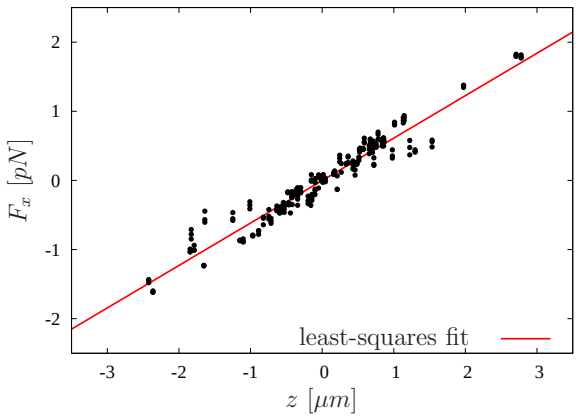

(b)

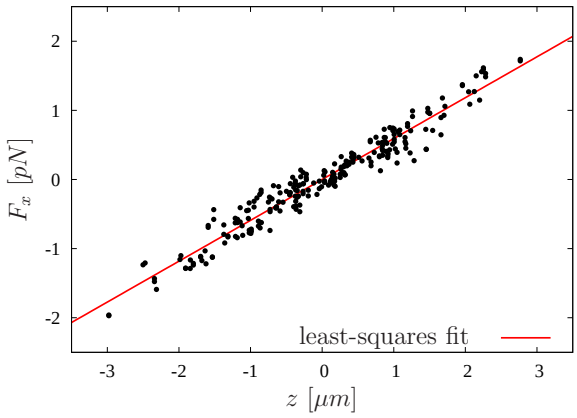

(c)

Figure 4: Distribution of drag inside of the small aggregates along the velocity gradient. Aggregates contain 8 particles each and the plots show the results for 10 different aggregates under 3 different angles of attack (30 data sets). Plots (a), (b) and (c) contain the data for the three aggregate types with sticking efficiencies of 1.00, 0.10 and 0.01, respectively.

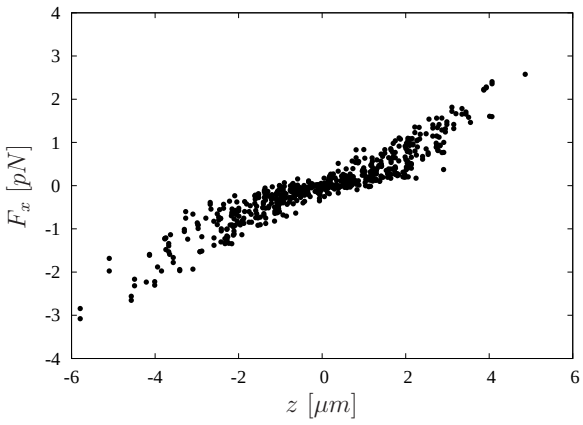

(a)

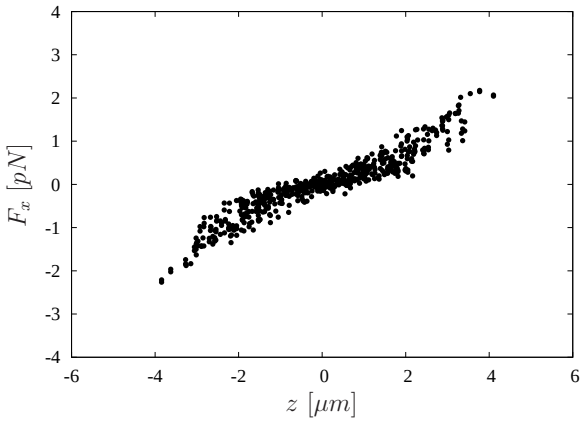

(b)

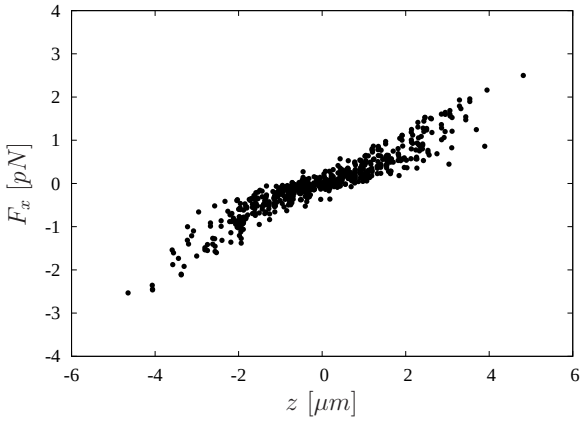

(c)

Figure 5: Distribution of drag inside of the larger aggregates along the velocity gradient. Aggregates contain 20 particles each and the plots show the results for 10 different aggregates under 3 different angles of attack (30 data sets). Plots (a), (b) and (c) contain the data for the three aggregate types with sticking efficiencies of 1.00, 0.10 and 0.01, respectively.

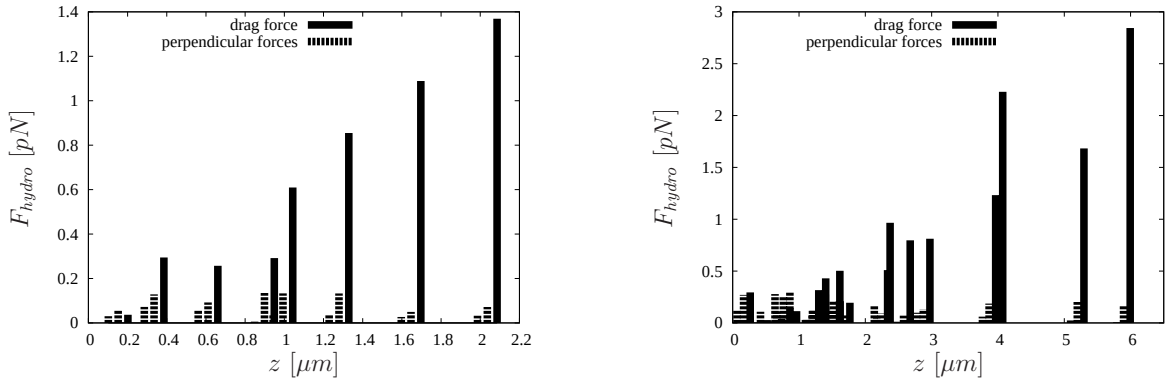

(a) (b)

Figure 6: Force components acting on the constituents of (a) an 8-particle, and (b) a 20-particle aggregate, $\epsilon = 1.00$. The absolute values are shown. The drag forces on the primary particles are dominant in the outer regions as expected but the perpendicular forces cannot be neglected for particles in the core region.

6 CONCLUSIONS AND OUTLOOK

High-resolution simulations offer insights into the hydrodynamic forces acting inside colloidal aggregates. The computational domain can be kept small in case of shear flow environments; this way, simulations of aggregates with up to 20 constituent particles become feasible. The differences between aggregates of different compactness are not significant and we attribute this to the fact that the structures under consideration were comparatively small. Based on simulations of two sizes of aggregates, the following conclusions can be drawn: First, the effective shear rate inside the aggregates is lower than the applied one. This means, that the flow inside the aggregate is shielded from the external flow. Moreover, the core region of the large aggregates is shielded more efficiently by the outer particles, and we expect this effect to be stronger for even larger aggregate structures. Second, the force components perpendicular to the outer flow are important for the modeling of the core region of both sizes of aggregates.

We propose that the hydrodynamic forces inside aggregates immersed in a shear flow environment should be described by effective shear rates, and for aggregates with 20 and more primary particles, a core-shell model with respect to the velocity gradient should be introduced into the mechanistic model in order to replace the free draining approximation.

ACKNOWLEDGMENTS

This work was supported by the German Research Foundation (DFG) within the framework of SPP 1273 priority program. Computing resources were provided in part by the AICES graduate school GSC 111 and the Forschungszentrum Jülich.

REFERENCES

[1] V. Becker and H. Briesen, Tangential-force model for interactions between bonded colloidal particles, *Physical Review E*, **78**, 061404 (2008).

[2] V. Becker, E. Schlauch, M. Behr, H. Briesen, Restructuring of colloidal aggregates in shear flows and limitations of the free-draining approximation, *J. Colloid and Interface Science*, **2**, 362–372 (2009).

[3] M. Behr and D. Arora, Shear-Slip Mesh Update Method: Implementation and Applications, *Computational Methods in Biomechanics and Biomedical Engineering*, **6**, 113–123 (2003).

[4] M. Behr and T.E. Tezduyar, Finite element solution strategies for large-scale flow simulations, *Computer Methods in Applied Mechanics and Engineering*, **112**, 3–24 (1994).

[5] M. Behr and L. P. Franca and T. Tezduyar, Stabilized Finite Element Methods for the Velocity-Pressure-Stress Formulation of Incompressible Flows, *Computer Methods in Applied Mechanics and Engineering*, **104**, 31–48 (1993).

[6] J. F. Brady, Stokesian Dynamics, *Annual Review of Fluid Mechanics*, **20**, 111–157 (1988).

[7] D. Chen and M. Doi, Simulation of aggregating colloids in shear flow, *Journal of Chemical Physics*, **91**, 2656–2663 (1989).

[8] D. Chen and M. Doi, Microstructure and Viscosity of Aggregating Colloids under Strong Shearing Force, *Journal of Colloid and Interface Science*, **212**, 286–292 (1999).

[9] M. Doi and D. Chen, Simulation of aggregating colloids in shear flow, *Journal of Chemical Physics*, **90**, 5271–5279 (1989).

[10] M. Elimelech, J. Gregory, X. Jia, R. A. Williams, *Particle Deposition and Aggregation Measurement: Modelling and Simulation*, **Elsevier**, Amsterdam (1948).

[11] M. Fanelli, F. L. Feke, I. Manas-Zloczower, Prediction of the dispersion of particle clusters in the nano-scale, *Chemical Engineering Science*, **61**, 4944–4956 (2006).

[12] M. Fanelli, F. L. Feke, I. Manas-Zloczower, Prediction of the dispersion of particle clusters in the nano-scale - Part I: Steady shearing responses, *Chemical Engineering Science*, **61**, 473–488 (2006).

[13] S. Harada, R. Tanaka, H. Nogami, M. Sawada, Dependence of fragmentation behavior of colloidal aggregates on their fractal structure, *Journal of Colloid and Interface Science*, **301**, 123–129 (2006).

[14] K. Higashitani, K. Iimura, H. Sanda, Simulation of deformation and breakup of large aggregates in flows of viscous fluids, *Chemical Engineering Science*, **56**, 2927–2938 (2001).

[15] Landau and Lifschitz, Lehrbuch der theoretischen Physik, Band VI Hydrodynamik, 5th Edition, *Akademie Verlag Gmbh* (1993).

[16] A. A. Potanin, On the modeling of colloid aggregates and aggregating colloids, *Journal of Chemical Physics*, **96**, (1992).

[17] A. A. Potanin, On the Computer Simulation of the Deformation and Breakup of Colloidal Aggregates in Shear Flow, *Journal of Colloid and Interface Science*, **157**, 399–410 (1993).

[18] A. Sierou and J. F. Brady, Accelerated Stokesian Dynamics simlations, *Journal of Fluid Mechanics*, **448**, 115–146 (2001).

[19] T. A. Witten and L. M. Sander, Diffusion-limited aggregation, a kinetic critical phenomenon, *Physical Review Letters*, **47**, 1400–1403 (1981).